Aeolian Erosion of Filled Martian Craters

M. D. Day[1], G. A. Kocurek[1], W. Anderson[2], A. M. Hamed[3], K. T. Christensen[3]

[1]University of Texas at Austin (mdday@utexas.edu), [2]Baylor University, [3]University of Illinois at Urbana Champaign.

Background

Craters are the dominant sedimentary basins on Mars. These topographic depressions provide immediate accommodation space for sediment influx and often house layered strata [1]. Many of these layered deposits are interpreted to be horizontally bedded units that do not extend across the entire basin floor [2]. Among these, Gale Crater contains an approximately 5 km high layered mound. Based on orbital observations, Malin and Edgett, 2000 hypothesized that intracrater layered deposits erode predictably from flat, to pitted, to mounded, and eventually to small isolated buttes. This study proposes that long-term aeolian deflation could give rise to the spectrum of crater fill described by above.

Aeolian processes have been recognized as important to the erosion of the surface of Mars for decades [3]. With liquid water unstable on the Martian surface, wind becomes the main driver of sediment transport [5]. Dunes, ventifacts, regs, and yardangs litter the surface of Mars and can be used to infer wind directions over time. More broadly, landscape evolution on Mars, including the formation of inverted topography and removal of strata, can be attributed to aeolian processes in the absence of water.

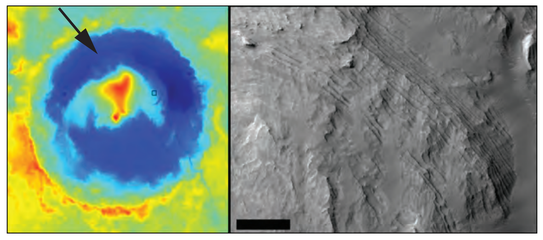

Figure 1: Partially filled Gale Cater with interior layered deposit. North is up. A) DEM of Gale Crater and its interior ~ 5 km high central layered mound. The black box indicates the approximate position of B). Gale Crater is ~155 km across. B) HiRISE image of layered strata in Gale's central mound. Scale bar is 500 m. Arrow indicates paleo-flow direction [10]. ESP_026291_1750.

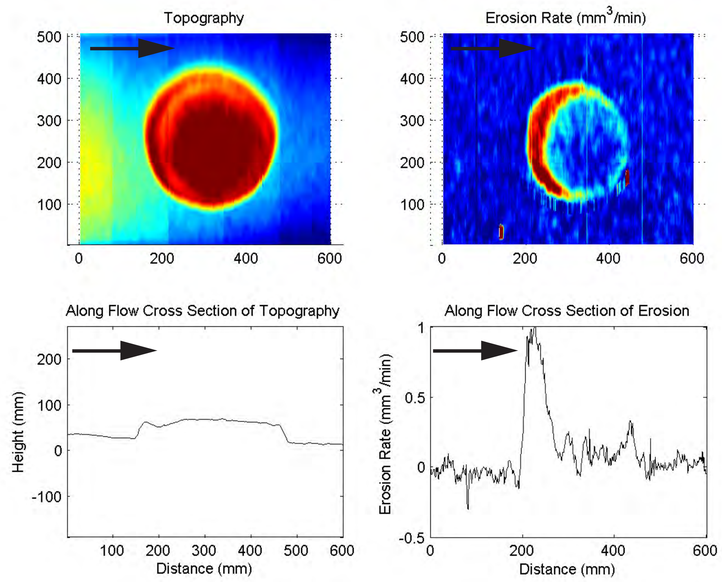

Figure 2: Snapshot of topographic evolution and differential erosion rates observed in wind tunnel experiments. Left hand plots show plan view digital elevation model of the crater (top) and centerline cross section cut in the direction of the flow (bottom). Right hand plots show contour map of erosion rate (top) and centerline cross section of erosion rate. Flow is left to right, indicated by arrows.

Wind Tunel Modeling

A series of physical models were constructed to capture the topography of an idealized crater. Filled with fine sand, these crater models were subjected to a constant unidirectional wind, and their loss of fill monitored until empty. Like the LES models, the physical models were restricted to 1:10 depth-to-diameter ratios. Water was added to the sand at a ratio of approximately 1:7 in order to increase the cohesion of the modeled crater fill. Digital elevation models of the modeled crater and its interior were taken every two minutes during the experiment to quantitatively analyze the amount, location, and rate of material lost. Experiments show a well-defined erosion pattern develops from high erosion rated along the rim interior that leads to formation of an interior mound.

Large Eddy Simulation

We conducted a series of LESs on a variety of modeled ideal crater topographies. Generated via superimposed Gaussian curves, the model crater topography was restricted to have a 1:10 depth-to-diameter ratio, as typical of fresh simple craters. Two stages of crater fill were tested: 100% fill and 90% fill (10% deflation). Crater models were all symmetrical, thus the chosen wind direction was arbitrary. Results indicate that helical vortices develop along the interior rim of the crater. We interpret these vortices and increased stresses to be the cause of high erosion rates observed in wind tunnel experiments.

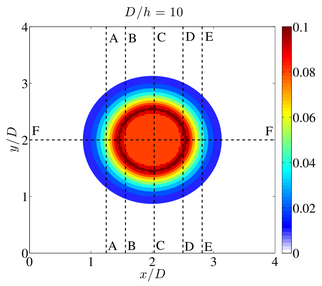

Figure 3: Digital elevation model used in LES with 10% interior deflation of fill. Cross section traces correspond to plots in Figure 5.

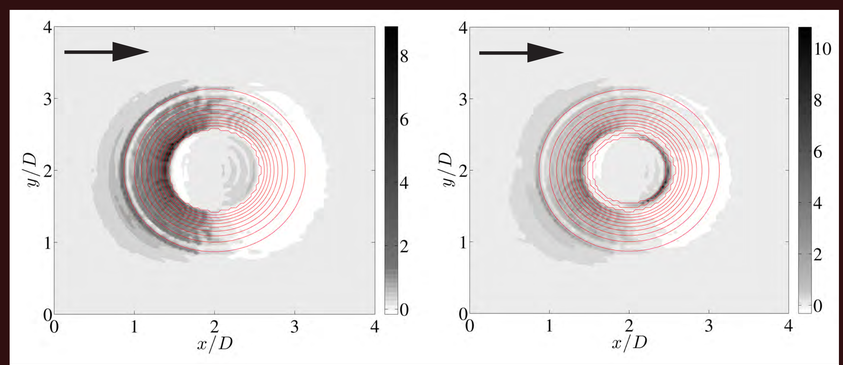

Figure 4: Contour map of aerodynamic drag on crater surface. Left: no deflation. Right: 10% deflation of interior. Arrows indicate flow direction

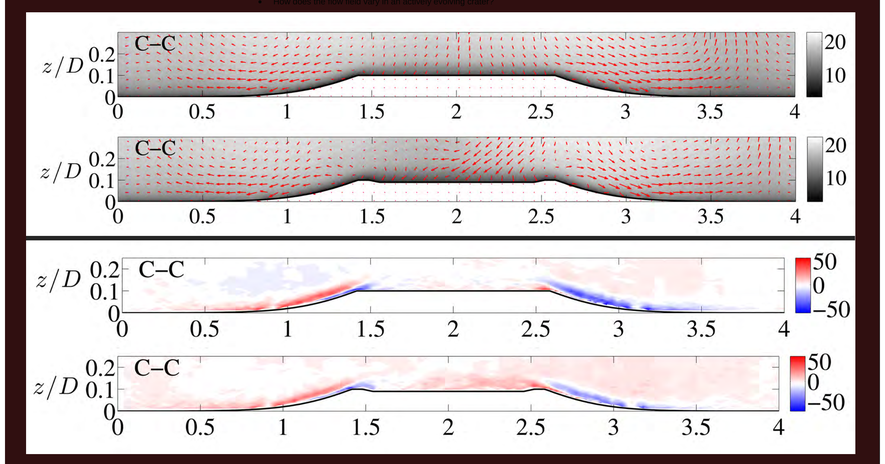

Figure 5: (Top) Centerline cross sections showing contour maps of time-averaged streamwise velocity with superimposed red vectors of time-averaged transverse and vertical velocity in y-z plane, and time averaged streamwise vorticity in y-z plane.
(Bottom) Progressive cross sections showing breakdown of time-averaged streamwise vorticity across the craters. Planes are denoted in the upper left and correspond to Figure 3 with the observer looking upwind.

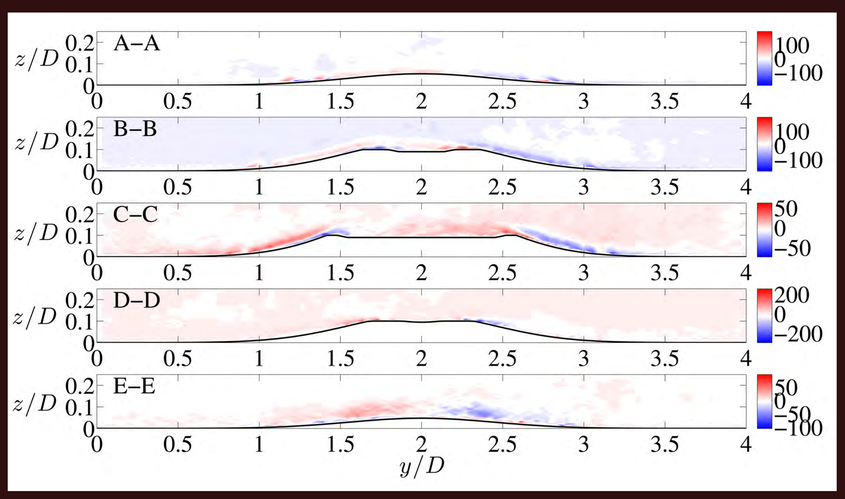

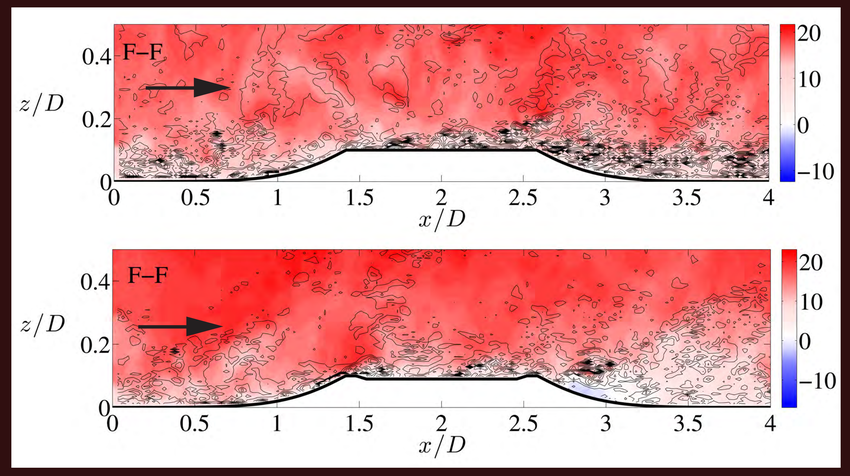

Figure 6: Contour map of instantaneous streamwise velocity with superimposed black contours of instantaneous transverse vorticity along F-F plane (x-z plane). Top: no deflation. Bottom: 10% deation of interior. Arrows indicate flow direction.

Future Work

Future work will focus on answering the following questions:

- **How do these results vary for complex craters?**
- **How does the flow field vary in an actively evolving crater?**

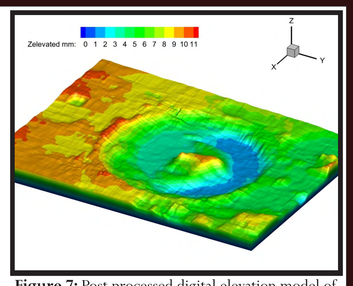

Figure 7: Post processed digital elevation model of Gale Crater used in the RIM facility. 3x vertical exaggeration.

Refractive Index Matching:

The flow over an acrylic model of the Gale Crater is currently under study using particle-image velocimetry (PIV) along with the refractive index matching (RIM) technique. Using the RIM technique grants full optical access to the model allowing for high-resolution measurements of the flow field over the crater. Spatial filtering was performed on the original DEM to mitigate the small scale roughness in the terrain of the crater.

Figure 8: The Refractive Index Matching (RIM) facility at University of Illinois and Urbana-Champaign is designed to model geophysical flows and can control sediment recirculation, temperature, and slope. Left: Photo of laboratory facility. Right: Schematic of laboratory setup.

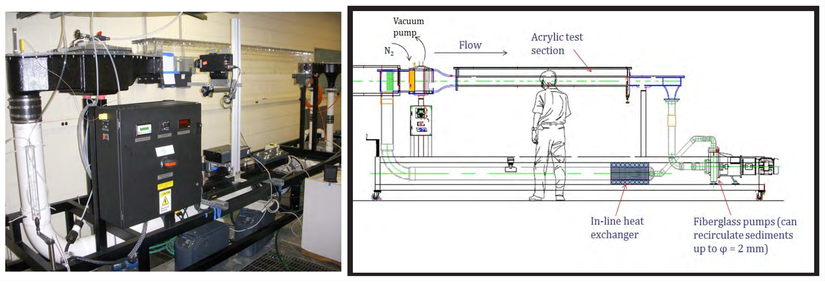

References:

[1] Malin, M. C. and Edgett K. S. (2000) Science, 290, 1927-1937. [2] DeLano K. and Hynek B. M. (2011) LPSC XLII Abstract # 2636. [3] Arvidson, R. E. et al. (1979) Nature, 278, 533-535. [4] Kok J. F. (2010) GRL, 37, L12202. [5] Wang Z. T. et. al. (2011) Phys. Rev. E., 84, 031304. [6] Edgett K. S. and Malin M. C. (2000) Geophys. R. Planets, 105, 1623-1650. [7] Wray J. J. (2013) Int. J. Astrobio., 12, 25-38. [8] Kite E. S. et al. (2013) Geology, 41, 543-546. [9] Rafkin S. C. R. (2001) Icarus, 151, 228-256. [10] Hobbs S. W. (2010) Icarus, 210, 102-115.

Acknowledgments:

Computational resources were provided by Academic and Research Computing Services at Baylor University and the Texas Advanced Computing Center at the University of Texas at Austin. This material is based upon work supported by the National Science Foundation Graduate Research Fellowship Program. Any opinions, findings, and conclusions or recommendations expressed in this material are those of the authors and do not necessarily reflect the views of the National Science Foundation. The development of the RIM facility was funded under NSF grant award CBET-0923106.